The Pharmacogenomics Journal (2011), 1–14
© 2011 Macmillan Publishers Limited. All rights reserved 1470-269X/11
www.nature.com/tpj

ORIGINAL ARTICLE

Characterization of the melanocortin-4-receptor nonsense mutation W16X *in vitro* and *in vivo*

F Bolze[1], N Rink[1], H Brumm[2], R Kühn[3], S Mocek[1], A-E Schwarz[1,4], C Kless[1], H Biebermann[2], W Wurst[3,5,6,7], J Rozman[1,4] and M Klingenspor[1]

[1]*Technische Universität München, Molecular Nutritional Medicine, Else Kröner-Fresenius Center and ZIEL-Research Center for Nutrition and Food Science, Freising, Germany;* [2]*Institute of Experimental Pediatric Endocrinology, Charité-Universitätsmedizin Berlin, Berlin, Germany;* [3]*Institute of Developmental Genetics, Helmholtz Zentrum München, German Research Center for Environmental Health (GmbH), Neuherberg/München, Germany;* [4]*Institute of Experimental Genetics, Helmholtz Zentrum München, German Research Center for Environmental Health (GmbH), Neuherberg/München, Germany;* [5]*Max Planck Institute of Psychiatry, München, Germany;* [6]*Technische Universität München, Chair of Developmental Genetics, Neuherberg/München, Germany and* [7]*DZNE, Deutsches Zentrum für Neurodegenerative Erkrankungen, LMU, Ludwig Maximilian Universität, Adolf Butenandt-Institut für Biochemie, München, Germany*

Correspondence:
Dr F Bolze, Technische Universität München, Molecular Nutritional Medicine, Else Kröner-Fresenius Center and ZIEL-Research Center for Nutrition and Food Science, Gregor-Mendel-Straße 2, Freising 85350, Germany.
E-mail: bolze@wzw.tum.de

Received 23 February 2011; revised 25 July 2011; accepted 1 September 2011

Several genetic diseases are triggered by nonsense mutations leading to the formation of truncated and defective proteins. Aminoglycosides have the capability to mediate a bypass of stop mutations during translation thus resulting in a rescue of protein expression. So far no attention has been directed to obesity-associated stop mutations as targets for nonsense suppression. Herein, we focus on the characterization of the melanocortin-4-receptor (*MC4R*) nonsense allele W16X identified in obese subjects. Cell culture assays revealed a loss-of-function of $Mc4r^{X16}$ characterized by impaired surface expression and defect signaling. The aminoglycoside G-418 restored $Mc4r^{X16}$ function *in vitro* demonstrating that $Mc4r^{X16}$ is susceptible to nonsense suppression. For the evaluation of nonsense suppression *in vivo*, we generated a $Mc4r^{X16}$ knock-in mouse line by gene targeting. $Mc4r^{X16}$ knock-in mice developed hyperphagia, impaired glucose tolerance, severe obesity and an increased body length demonstrating that this new mouse model resembles typical characteristics of *Mc4r* deficiency. In a first therapeutic trial, the aminoglycosides gentamicin and amikacin induced no amelioration of obesity. Further experiments with $Mc4r^{X16}$ knock-in mice will be instrumental to establish nonsense suppression for *Mc4r* as an obesity-associated target gene expressed in the central nervous system.
The Pharmacogenomics Journal advance online publication, 4 October 2011; doi:10.1038/tpj.2011.43

Keywords: melanocortin-4-receptor; obesity; nonsense suppression; aminoglycosides

Introduction

Nonsense mutations cause a premature termination of protein biosynthesis and can disable the proper function of a gene. Approximately 10% of cases in human inherited diseases such as cystic fibrosis, diabetes insipidus, Hurler syndrome and muscle dystrophy are the consequence of nonsense mutations.[1–4] Several *in vitro* and *in vivo* studies have demonstrated that aminoglycosides like amikacin, gentamicin and G-418 have the ability to suppress clinically relevant stop mutations leading to a fractional reactivation of protein expression and function.[5–8] It is hypothesized that aminoglycosides bind to the ribosome and lower the accuracy of codon–anticodon interaction thus allowing the incorporation of a random amino acid at the mutated position.[9] Read-through of nonsense mutations depends on the sequence of the termination codon. In general, highest suppression efficiencies were demonstrated for the TGA codon, followed by TAG and TAA.[6,8] In addition, the nucleotide context surrounding the stop signal affects suppression efficiencies.[6,8] Beside the lack of oral bioavailability, the clinical application of aminoglycosides is limited because of adverse effects, including oto- and nephrotoxocity.[10,11] Other non-aminoglycoside nonsense

suppressors, like the oxadiazol compound PTC124 (Ataluren), or the peptide antibiotic negamycin with mild side effects might be alternative means of establishing nonsense suppression in humans.[12–14]

Obesity has become a major health concern in the last decades since an excess body fat accumulation is often accompanied by complex disease traits like cardiovascular disorders, type 2 diabetes and certain forms of cancer.[15] Body weight is influenced by extensive interactions among environmental, psychosocial and genetic factors.[16] So far no attention has been addressed to obesity-associated nonsense mutations as targets for stop suppressor compounds. Several stop mutations were identified in genes that are critical for the hypothalamic control of energy balance. Premature stop codons in genes encoding prohormone convertase 1, leptin receptor, pro-opiomelanocortin (*POMC*) and melanocortin-4-receptor (*MC4R*) were identified in obese subjects demonstrating the impact of certain nonsense alleles on energy homeostasis.[17–20]

Herein, we focus on the characterization of the *MC4R*^{X16} gene variant, which was identified in two obese females heterozygous for the stop mutation.[21] A single-nucleotide substitution (G→A) changes the highly conserved tryptophan encoding triplet TGG to a premature TGA termination codon. In addition to W16X, further stop mutations exist in the human *MC4R* gene. The non-conserved Y35X (TAA) as the most common *MC4R* stop variant exhibits heterozygous genotype frequencies around 0.5% in obese people.[22]

The MC4R is a 332 amino acid G-protein-coupled receptor mainly expressed in hypothalamic nuclei involved in the regulation of energy balance.[23] The naturally occurring MC4R agonist α-melanocyte-stimulating hormone (MSH) is generated by post-translational processing of the protein precursor POMC.[24] Activation of MC4R-signaling induces a reduction in energy intake and an elevation of energy expenditure thus resulting in negative energy balance and weight loss.[25,26] The physiological importance of MC4R is demonstrated by several obese mouse models harboring loss-of-function mutations in the *Mc4r* locus.[27,28] Furthermore, *MC4R* mutations have turned out to be the most frequent cause for monogenic obesity since approximately 150 variants including frameshift, missense and nonsense mutations have been predominately detected in obese individuals.[29] In our report, we investigated whether the MC4R^{X16} is a target for nonsense suppression. In cell cultures overexpressing *Mc4r*^{X16}, we applied the aminoglycoside G-418 and assessed plasma membrane expression and signaling properties. Very recently, Mul *et al*.[30] published an obese *Mc4r*^{K314X} rat model suitable for the *in vivo* evaluation of stop suppression. But so far, existing mouse lines carrying missense mutations or insertion cassettes in the *Mc4r* gene are not appropriate to evaluate the efficiency of nonsense mutation suppressors. To generate an adequate model for our therapeutic intention, we inserted the W16X nonsense mutation into the murine *Mc4r* locus by gene replacement. Before conducting a large study to examine the effect of putative stop suppressors, we performed metabolic phenotyping of *Mc4r*^{X16} knock-in mice to ascertain whether this animal model exhibits characteristics that are in concordance with other *Mc4r*-deficient mouse lines. Furthermore, we tested in a first approach the potent nonsense suppressors gentamicin and amikacin *in vivo* and monitored body weight and food consumption of the *Mc4r*^{X16} knock-in mouse line.

Materials and methods

Functional characterization of Mc4r^{X16} in vitro

The murine *Mc4r*^{wt} (NM_016977) and *Mc4r*^{X16} open reading frames were PCR amplified and inserted into the eukaryotic expression vectors pcDps and pcDNA4 (Invitrogen, Karlsruhe, Germany), respectively. The W16X mutation was labeled 5-bp downstream with a silent mutation generating a *Xho*I restriction site. pcDNA4 constructs contained the nucleotide sequence for an N-terminal express epitope tag for enzyme-linked immunosorbent assay-based quantification of cell surface expression. pcDps constructs were employed for the functional analysis in a cyclic adenosine monophosphate (cAMP) accumulation assay.

For investigation of agonist-dependent cAMP accumulation, Cos7 cells were seeded in 12-well plates (2×10^5 cells per well) on the day before transfection. Cells were transfected with 1.5 μg DNA per well of expression vectors either encoding *Mc4r*^{wt} or *Mc4r*^{X16} gene by lipofection in accordance to the manufactures instructions (Metafectene, Biontex, Martinsried, Germany). On the day after, the transfection cells were coincubated for 24 h with 75 μg ml^{-1} G-418 (Invitrogen) and ^{3}H-Adenin (Perkin Elmer, Boston, MA, USA). Cells were stimulated for 1 h with various concentrations of α-MSH and NDP-α-MSH respectively along with the phosphodiesterase inhibitor 1 mM isobutylmethylxanthine (Sigma, Deisenhofen, Germany). The reaction was stopped by adding cold trichloroacetic acid to the cells. ^{3}H-cAMP was purified using Dowex AG 1-X8-columns (Bio-Rad, Hercules, CA, USA). Radioactivity was assessed and receptor activity is expressed as counts per well. Sigmoidal dose response curves were generated using Prism 4 software (GraphPad, La Jolla, CA, USA).

For assessment of cell surface expression, HEK293 cells were seeded in 12–well dishes (6×10^5 cells per well) coated with 0.1% (w/v) poly-D-lysine on the day before the transfection. Cells were transiently transfected with 2.5 μg *Mc4r* expression vector per well utilizing the calcium phosphate method (Profection, Promega, Mannheim, Germany) in concordance to the manufacturer's instructions. On the day after, the transfection cells were treated with 75 μg ml^{-1} G-418 (Invitrogen) for 24 h. After washing the cells with phosphate-buffered saline (PBS) containing 0.1% bovine serum albumin (BSA), cells were fixed in 4% formaldehyde in PBS. Then cells were washed twice with PBS containing 0.1% BSA to remove residual formaldehyde. After blocking unspecific protein-binding sites with PBS containing 1% BSA, Xpress epitope tagged MC4R fusion proteins were detected by incubating cells with 1/2500 diluted mouse-derived anti-Xpress antibody (Invitrogen) in PBS containing 0.1% BSA. Cells were washed twice with PBS containing 0.1% BSA and blocked with PBS containing 1%

BSA. Then cells were incubated with 1/2500 diluted secondary anti-mouse antibody from goat (Dianova, Hamburg, Germany) conjugated with horseradish peroxidase in PBS containing 0.1% BSA. Afterward cells were washed three times with PBS containing 0.1% BSA. The peroxidase substrate o-phenylenediamine dihydrochlorid (Sigma) was used in accordance to the manufacturer's instructions. After 10–15 min, the reaction was terminated by adding 3 N HCl. Optical density was assessed at 492 nm in a photometer.

Generation of Mc4r^{X16} knock-in mice

The two homology arms for the *Mc4r*^{X16} targeting vector were PCR amplified utilizing a C57BL/6J BAC clone (RP24-566k) as template. (Primers for the *Mc4r* exon bearing 5′ arm of homology: *forward* 5′-GATCGCGCCCGCTCGCCATTGG AGAAAGTGTGAAAAG-3′; *reverse* 5′-CATGGGCGCGCCGG AACCAGATCCCTGGTAAGAAGCC-3′.) The nonsense mutation at codon 16 (TGG→TGA) was introduced into the *Mc4r* exon by site-directed mutagenesis (Mutagenesis primers: *forward* 5′-CTTCCCTCCACCTCTGAAACCGCTCGAGCTAC GG-3′; *reverse* 5′-CCGTAGCTCGAGCGGTTTCAGAGGTGGA GGGAAG-3′). For simplified genotyping, a silent mutation generating a *Xho*I restriction site was additionally inserted 5-bp downstream of the W16X mutation. (Primers for the 3′ arm of homology: *forward* 5′-TAGCGGCCGGCCTACAGA AAGGTCTAGAACAGCTCCC-3′; *reverse* 5′-ATGCCTCGAGAA GATATTTCATGGGGACAGGGGAGAG-3′.)

The PCR products were cloned into the pEasyFloxII targeting vector providing a *loxP* flanked *neomycin resistance* gene (*neo*). A viral thymidine kinase negative selection marker was localized downstream of the 3′ arm of homology. The targeting construct was verified by DNA sequencing.

The targeting vector was electroporated into F1 V6.5 embryonic stem (ES) cells, which were derived from breeding C57BL/6J with 129SvJae mice.[31] To enrich ES cells bearing the targeting construct selection with 140 μg ml^{-1} G-418 and 2 mM Gancyclovir was started 2 and 5 days subsequently after the transfection, respectively. Correct gene targeting was confirmed by Southern blotting using a 644-bp PCR fragment (primers: *forward* 5′-GTATTTTGCT TTGAGGGACTTGAG-3′; *reverse* 5′-ATTGGTGGCCTTTAGAT TGATG-3′). The presence of the mutation was verified by PCR-based amplification of the adequate region and *Xho*I restriction digest of the PCR product (primers: *forward* 5′-CTACAGGCATACAGACTGGGAG-3′; *reverse* 5′-GTACATG GGTGAGTGCAGGTTC-3′).

Recombinant ES cells were injected into C57BL/6J blastocysts and then implanted into pseudo-pregnant female mice. Chimeric F0 progeny carrying agouti fur color were bred with C57BL/6J mice to confirm germ line transmission of the *Mc4r*^{X16} allele in F1 mice. Mice carrying *Mc4r*^{X16} were identified by detecting the *Xho*I site. Additionally, sequencing affirmed the presence of the nonsense mutation. To minimize side effects of the loxP flanked neomycin gene heterozygous F1 mice were crossed with C57BL/6-*Gt(ROSA) 26Sor tm16(Cre)Arte* (Taconic Artemis, Cologne, Germany) to eliminate the selection marker from the genome. The remaining sequence after the neomycin deletion (34 bp from the loxP-site and 112 bp from the poly linker) allowed PCR-based discrimination between the *Mc4r*^{wt} and *Mc4r*^{X16} allele (primers: *forward* 5′-CCTATGCCAAATGATACCCCA CC-3′; *reverse* 5′-CTCTAAGATGAAATGAACGCTGGACC-3′). Heterozygous mice were bred to produce mice of all three genotypes for metabolic phenotyping. Standard genotyping of mice was performed by detecting the additional *Xho*I recognition site and by the remaining *loxP* sequence as markers for the *Mc4r*^{X16} allele.

Animal housing

Experiments were performed with permission from the district government of Upper Bavaria (Regierung von Oberbayern) reference number Az.55.2-1-54-2531-90-08. Two different cohorts were used for metabolic phenotyping:

Cohort 1 (all experiments except indirect calorimetry). Mice were housed in a conventional open animal facility with pelleted food (type R/M-H, Ssniff: 58% energy from carbohydrate, 33% from protein and 9% from fat) and water *ad libitum* at 22 °C in a 12:12 h light–dark cycle. Animals were maintained in groups. Only when food intake was monitored mice were separated and singly housed for the duration of the experiment.

Cohort 2 (only indirect calorimetry). Mice were housed in a specific pathogen-free animal facility with pelleted food (type M/Z, Ssniff: 53% energy from carbohydrate, 36% from protein and 11% from fat) and water *ad libitum* at 22 °C in a 12:12 h light–dark cycle. Animals were singly housed for their whole life span.

Weight, length and body composition measurements

Weight development was monitored regularly beginning at the age of 21 days. Body length was measured in transiently chloroform-narcotized mice. Animals were carefully extended to their full length, always by the same experimenter and the snout-to-anus distance was determined. Abdominal body composition (*lumbar vertebra* 1–6) of dead animals was measured in a LaTheta micro computer tomography scanner (Aloka, Meerbusch, Germany). Adipose tissue was distinguished into visceral and subcutaneous fat depots.

Energy intake, energy assimilation and assimilation efficiency

For food intake measurements, animals were singly housed on plastic grids for 1 week. Mice were adapted for 3 days to the new environment. Afterward food intake was monitored for the next 4 consecutive days. At the end of the experiment, feces were collected and food consumption was corrected for spillage.

Food and feces samples were analyzed for their energy content in a bomb calorimeter (type 6300 Calorimeter, Parr, Frankfurt, Germany). Samples were dried in a heating cabinet until weight constancy. Afterward samples were homogenized and pressed to tablets. Energy intake (E_{in}), feces energy content (E_{out}), energy assimilation (E_{ass}) and assimilation efficiency were calculated as followed: E_{in} (kJ day^{-1}) = food intake (g day^{-1}) × energy content food

($kJ\,g^{-1}$); E_{out} ($kJ\,day^{-1}$) = feces production ($g\,day^{-1}$) × energy content feces ($kJ\,g^{-1}$); E_{ass} ($kJ\,day^{-1}$) = $E_{in} - E_{out}$; assimilation efficiency (%) = $E_{out}/E_{in} \times 100$.

Rectal body temperature
Rectal body temperature was assessed utilizing a precision thermometer (Almemo 2490, Ahlborn, Holzkirchen, Germany). Temperature of each individual was taken three times during 5 days and the mean value for each individual was calculated. The measurements were performed at the same time of day and by the same researcher.

Indirect calorimetry
Indirect calorimetry was performed in an open flow respiratory system to assess energy expenditure (Phenomaster, TSE Systems, Bad Homburg, Germany). Single mice were placed in metabolic cuvettes (volume ~2.5 l) with food and water *ad libitum* at 22 °C for 3 days. The first 24 h were considered as acclimatization and were excluded from the analysis. Extracted air from the cuvette (flow rate $30\,l\,h^{-1}$) was dried in a cooling trap and analyzed approximately every 6 min for O_2 and CO_2 content. Oxygen consumption, carbon dioxide production and energy expenditure were calculated as described previously.[32] Energy expenditure was calculated per hour. Values per hour were summated to assess daily energy expenditure.

Intraperitoneal glucose tolerance test
Before the glucose tolerance test mice were fasted for 6 h. Blood from the tail tip was analyzed with a whole blood monitor (FreeStyle Lite, Abbott, Wiesbaden, Germany) to determine blood glucose concentrations. Afterward mice received an intraperitoneal glucose load ($2\,g\,glucose\,kg^{-1}$ body weight). During the next 2 h blood was taken in regular intervals (15, 30, 60 and 120 min) for blood glucose determinations. The total area under the curve was calculated by using Prism 4 software (GraphPad).

Hypothalamic gene expression
Hypothalami were dissected with a brain blocker to achieve a standardized tissue sampling. Tissue was snap frozen in liquid nitrogen and stored at −80 °C until RNA purification. RNA was extracted using Trisure reagent (Bioline, Luckenwalde, Germany) and integrity was confirmed by gel electrophoresis. (None of the RNA samples were contaminated with genomic DNA tested by PCR.) RNA was reverse transcribed with the Quantitect cDNA synthesis kit (Qiagen, Hilden, Germany). Quantitative real-time PCR was performed utilizing a SYBR Green supplemented SensiMix (Bioline) in accordance to the manufacturer's instructions. The efficiency of amplification was calculated based on 2^n dilution series standard curves (Realplex Cycler software, Eppendorf, Hamburg, Germany) and used to determine starting quantity of the templates. The geometric mean of two housekeeping genes (*heat shock protein 90* and *β-actin*) was used for normalization of transcript quantities in each individual sample. The primer pairs listed in Table 1 were validated and used for quantitative reverse transcriptase-PCR.

Aminoglycoside treatment protocol
Treatment consisted of dorsal subcutaneous injections either of gentamicin (Hexal, $34\,mg\,kg^{-1}\,day^{-1}$) or amikacin (Sigma, 170 and $510\,mg\,kg^{-1}\,day^{-1}$) solved in PBS 1 h before lights off. In the pre-treatment phase, animals were adapted to the handling procedure with control injections. Hereafter, all animals were switched to the aminoglycoside treatment. Treatment protocols are detailed in the result section and the corresponding figure legends.

Results

Functional characterization of $Mc4r^{X16}$ in vitro
In a first approach, the plasma membrane expression of murine $MC4R^{wt}$ and $MC4R^{X16}$ was investigated in transiently transfected HEK293 cells using a surface enzyme-linked immunosorbent assay. The stop mutated variant $MC4R^{X16}$ showed no surface expression under control conditions compared with $MC4R^{wt}$ (Figure 1a). The administration of $75\,\mu g\,ml^{-1}$ G-418 induced a significant restoration of $MC4R^{X16}$ plasma membrane abundance whereas $MC4R^{wt}$ surface expression was unaffected by treatment (Figure 1a).

Cell signaling was characterized in a radiolabeled cAMP accumulation assay. In accordance to the surface enzyme-linked immunosorbent assay under control conditions, the $MC4R^{X16}$ showed a loss-of-function phenotype. The agonists α-MSH and NDP-α-MSH did not induce a remarkable cAMP production in $MC4R^{X16}$-expressing Cos7 cells (Figure 1b). In the presence of $75\,\mu g\,ml^{-1}$ G-418, the signaling properties of $MC4R^{X16}$-expressing cells in response to α-MSH and NDP-α-MSH were reactivated (Figure 1c). Taken together in cell culture experiments, the aminoglycoside G-418 caused a suppression of the obesity-associated stop mutation $Mc4r^{X16}$.

Table 1 Primer pairs for quantitative real-time PCR

Gene name	*Forward primer*	*Reverse primer*
β-Actin	5′-AGAGGGAAATCGTGCGTGAC-3′	5′-CAATAGTGATGACCTGGCCGT-3′
Heat shock protein 90	5′-AGGAGGGTCAAGGAAGTGGT-3′	5′-TTTTTCTTGTCTTTGCCGCT-3′
Agouti-related protein	5′-TCCCAGAGTTCCCAGGTCTAAGTC-3′	5′-GCGGTTCTGTGGATCTAGCACCTC-3′
Neuropeptide Y	5′-GGCAAGAGATCCAGCCCTG-3′	5′-CCAGCCTAGTGGTGGCATGC-3′
Proopiomelanocortin	5′-CCCTCCTGCTTCAGACCTC-3′	5′-CGTTGCCAGGAAACACGG-3′
Melanocortin-4-receptor	5′-CGTCATCGACCCTCTCATTT-3′	5′-CACAGAAGAGGCAGCTGTTG-3′

Generation of Mc4r^{X16} knock-in mice

A targeting construct on the basis of C57BL/6J DNA was generated to introduce the nonsense mutation W16X into the murine *Mc4r* gene. The vector consisted of two approximately 3.8 kb arms of homology flanking a loxP flanked neomycin resistance gene. Downstream of the 3′ homology arm a thymidine kinase gene for negative selection was placed. Ten days after electroporation, a total of 350 G-418 and ganciclovir double resistant ES cell clones were isolated and screened by Southern blot hybridization of *Eco*RI- and *Eco*RV-digested genomic ES cell DNA respectively with a *Mc4r* exon flanking probe (Figure 2a).

Wild-type and recombinant ES clones showed a different *Eco*RV restriction pattern in the Southern blot analysis. Five clones had the predicted 10.9 kb targeted *Eco*RV fragment in addition to a 23.6 kb fragment (Figure 2b). The latter band was unexpected because the *in silico* analysis based on the C57BL/6J genomic sequence led us anticipate a wild-type *Eco*RV fragment at 15.1 kb. The NCBI polymorphism database contains an A→G nucleotide exchange (rs29576391) disrupting the nearest upstream *Eco*RV recognition site (underlined in Figure 2a) of the 129SvJae *Mc4r* gene therewith leading to the larger band observed in the Southern blot hybridization. Furthermore, the polymorphism was experimentally confirmed after *Eco*RV-digest of PCR products utilizing C57BL/6J, 129SvEvTac and ES cell DNA as PCR template (data not shown).

An additional Southern blot strategy with *Eco*RI-digested ES cell DNA revealed the assumed fragment sizes of wild-type (10.8 kb) and recombinant (9.3 kb) *Mc4r* alleles (Figure 2c). The *Xho*I recognition site next to the W16X position allowed PCR/restriction digest-based identification of ES clones carrying the mutation of interest. One of five targeted clones was positive for the premature TGA codon (data not shown). Implantation of this clone into C57BL/6J blastocysts produced several F0-chimeras that, when mated with C57BL/6J mice, transmitted the mutated *Mc4r* gene to their F1-offspring. Heterozygous F1 males were crossed with *Rosa*-Cre deleter mice to eliminate the *loxP*-flanked *neo* gene from the targeted *Mc4r*^{X16} locus in the germ line. Successful *neo* deletion in F2 generation was demonstrated by PCR-based verification of the remaining *loxP* sequence. Further genotyping of F3 progeny used for the phenotyping experiments was performed by detecting the *loxP* site and the silent mutation causing a *Xho*I restriction site close to the W16X mutation (Figures 2d and e). Results for both genotyping strategies were always in concordance. Genotype distribution was in line with Mendelian inheritance. Sequencing confirmed the presence of the premature TGA codon in the *Mc4r* gene (Figure 2f).

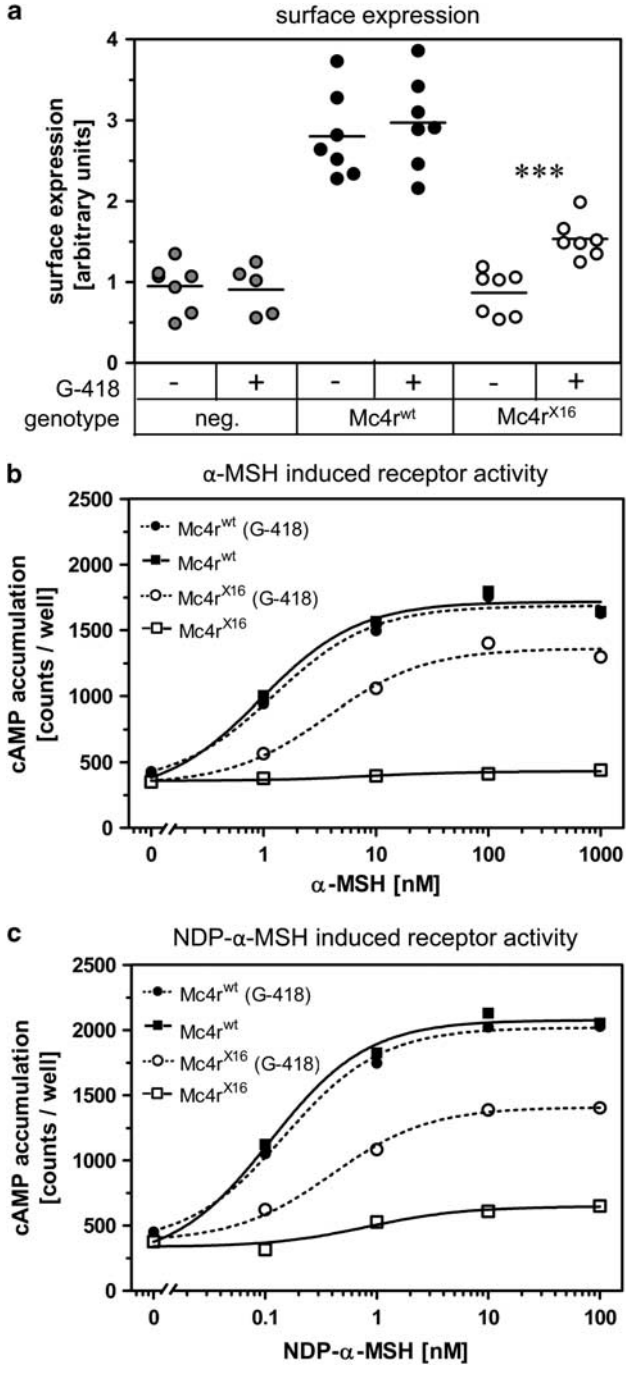

Figure 1 Aminoglycoside (G-418)-mediated restoration of *Mc4r*^{X16} *in vitro*. (**a**) HEK293 cells were transiently transfected with expression vectors either encoding *Mc4r*^{wt} or *Mc4r*^{X16}. Untransfected cells served as negative control (neg.). Before receptor quantification in the plasma membrane, cells were incubated with 75 μg ml^{-1} G-418 for 24 h. Abundances of Xpress–Mc4r fusion proteins were measured with a surface enzyme-linked immunosorbent assay (ELISA) utilizing an anti-Xpress antibody (***$P<0.001$; Mann–Whitney *U*-test). (**b**, **c**) Cos7 cells were transiently transfected with expression vectors either encoding *Mc4r*^{wt} or *Mc4r*^{X16}. Transfected cells were incubated with 75 μg ml^{-1} G-418 for 24 h or cultured the same time in aminoglycoside-free medium. A radioactive cAMP accumulation assay was used to assess α-melanocyte-stimulating hormone (MSH) and NDP-α-MSH induced receptor activity (shown is one representative experiment performed in replicates).

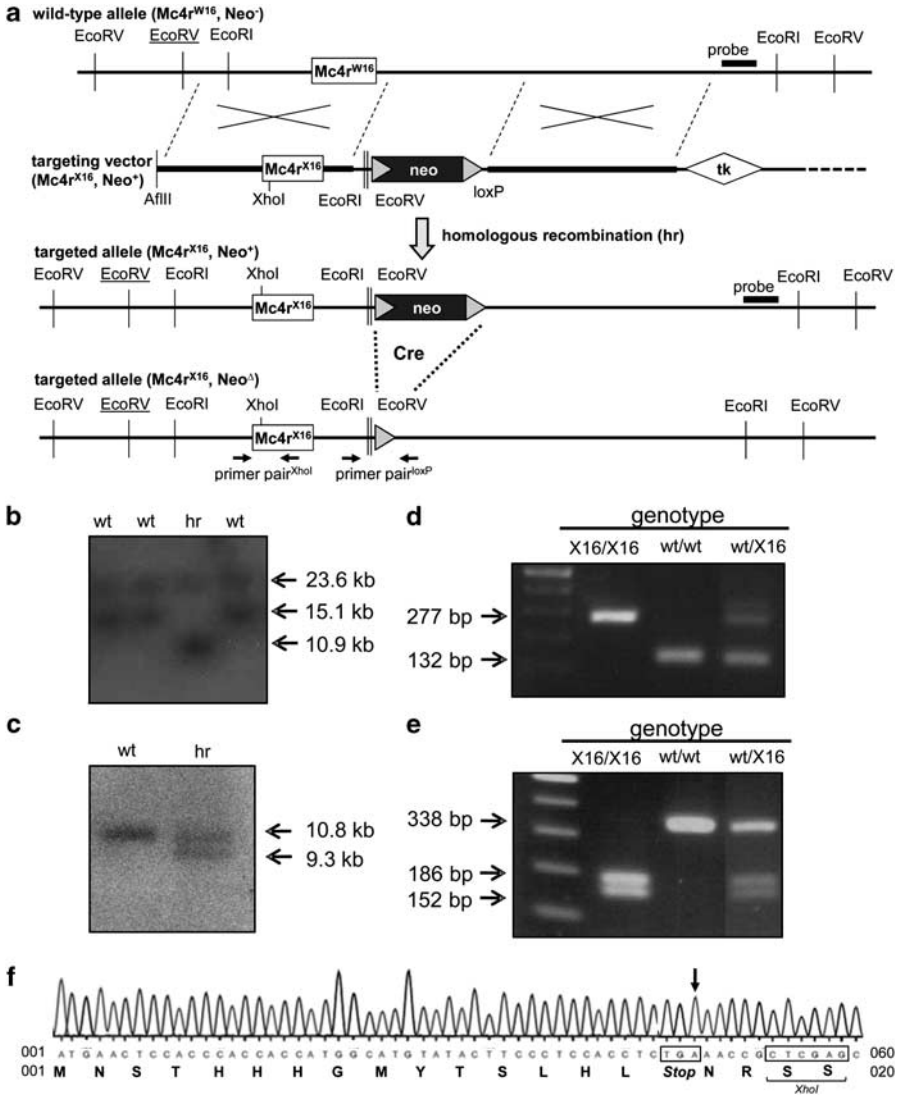

Figure 2 Generation of the *Mc4r*^{X16} knock-in mouse line. (**a**) *Afl*II linearized targeting vector consisting of two arms of homology, a neomycin resistance gene (neo) and a thymidin kinase gene (tk) was used for the electroporation of embryonic stem (ES) cells with a mixed C57BL/6J and 129SvJae genetic background. Additional *Eco*RI and *Eco*RV restriction sites provided by the targeting construct changed the fragment pattern of recombinant clones in a Southern blot analysis. For hybridization, a flanking DNA probe was applied. Neo gene was eliminated by Cre-mediated deletion using a Rosa-Cre mouse line *in vivo*. (**b**) Wild-type ES cells (wt) displayed a double band in the Southern blot because the 129SvJae Mc4r locus had an annotated polymorphism in one *Eco*RV (underlined in **a**) recognition site resulting in a fragment of 23.6 kb. Homologous recombination (hr) of the C57BL/6J allele resulted in the expected fragment size of 10.9 kb. (**c**) Further blotting of *Eco*RI-digested DNA additionally confirmed successful gene targeting. The wild-type *Eco*RI fragment had a length of 10.8 kb, the targeted allele showed a size of 9.3 kb. Cre/loxP-mediated elimination of the neomycin resistance gene was achieved by breeding heterozygous F1 Mc4r$^{X16/wt}$ knock-in mice with Rosa-Cre deleter mice. (**d**) Successful neo deletion was confirmed by PCR. The remaining polylinker/loxP sequence allowed the PCR-based discrimination between the *Mc4r*^{wt} (132 bp) and *Mc4r*^{X16} (277 bp) allele. (**e**) The presence of the premature TGA codon labeled with a silent mutation resulting in a *Xho*I site was confirmed by PCR enrichment of the adequate region and subsequent *Xho*I restriction digest. (**f**) Sequencing of the Mc4r gene of heterozygous F1 Mc4r$^{X16/wt}$ knock-in mice demonstrated the presence of the stop mutation. The silent mutation generating the *Xho*I recognition site was located 5-bp downstream of the premature termination codon.

Body weight, body composition and body length

At the age of around 6–7 weeks, *Mc4r*$^{X16/X16}$ knock-in mice of both sexes became obviously heavier than *Mc4r*$^{wt/wt}$ littermates. *Mc4r*$^{X16/wt}$ animals with one mutated *Mc4r* allele exhibited an intermediate body weight phenotype (Figures 3a and b). Male *Mc4r*$^{X16/X16}$ knock-in mice older than 6 month weighed 70% more than their wild-type litter mates. The effect strength of the W16X mutation was more pronounced in female mice since weight increase in *Mc4r*$^{X16/X16}$ females was nearly 100% in comparison with wild types.

Abdominal body composition of dead mice between 25 and 28 weeks of age was assessed by computer tomography. Increased body weight was mainly because of an increase in

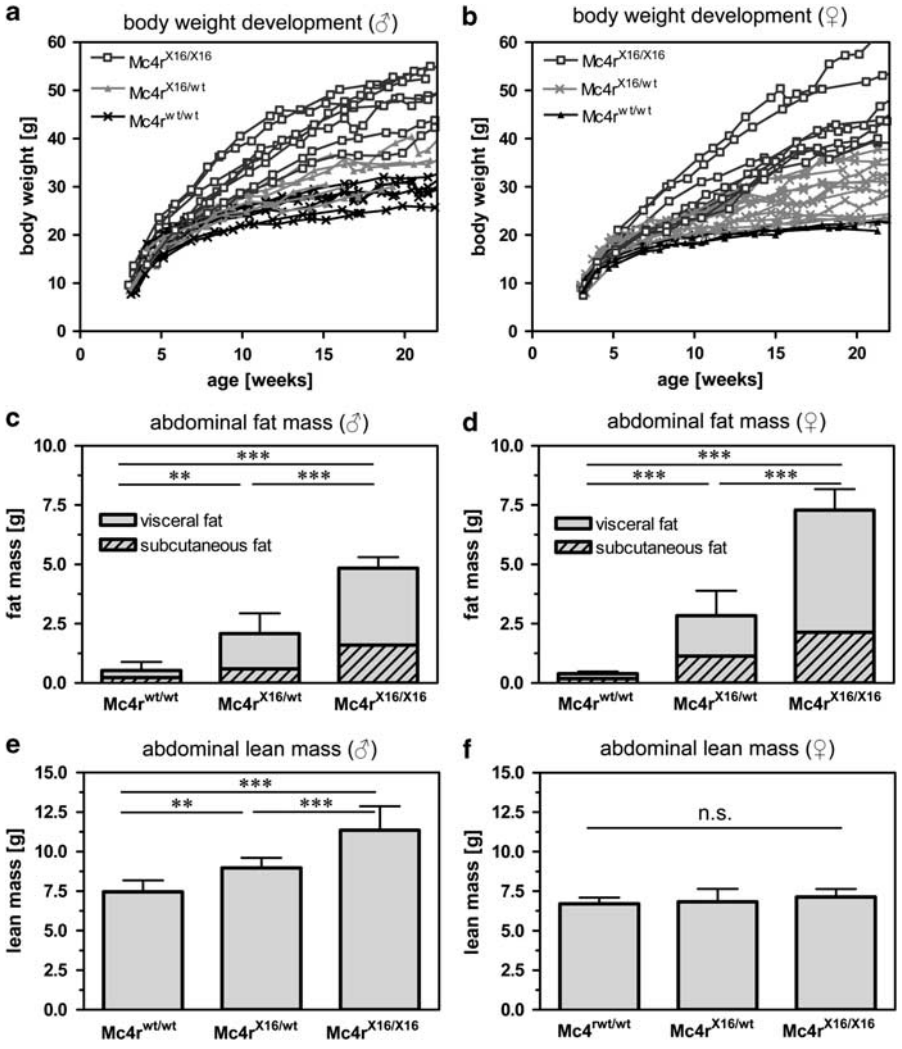

Figure 3 Weight development and abdominal body composition of the *Mc4r*^{X16} knock-in mouse line. Body weight development of males ($n=6$–8) (**a**) and females ($n=4$–10) (**b**). Each line represents the body weight of an individual mouse. Body composition was determined with a computer tomography device in the age of 25–28 weeks. Abdominal fat mass of male ($n=6$–11) (**c**) and females ($n=6$–10) (**d**) mice. Each column represents the mean value with s.d. The uniform area displays visceral fat, the striped area the subcutaneous fat. Abdominal lean mass for male ($n=6$–11) (**e**) and female ($n=6$–10) (**f**) mice. (**$P<0.01$; ***$P<0.001$, one-way analysis of variance (ANOVA) and Holm–Sidak *post-hoc* test).

visceral fat tissue (Figures 3c and d). In line with the body weight data, heterozygous *Mc4r*$^{X16/wt}$ mice showed a gain in fat mass intermediate to that observed in *Mc4r*$^{X16/X16}$ and *Mc4r*$^{wt/wt}$ mice. Beside the elevated fat mass, a sex-specific difference in lean mass was detected. Only male *Mc4r*$^{X16/X16}$ mutants showed a higher lean mass than *Mc4r*$^{X16/wt}$ and *Mc4r*$^{wt/wt}$ littermates (Figures 3e and f). In the second mice cohort used for the assessment of energy expenditure, animals were singly housed under specific pathogen-free conditions. Here, lean mass in *Mc4r*$^{X16/X16}$ mice of both sexes was reduced compared with wild types (data not shown).

To examine whether mutant mice possessed abnormalities in body length, snout-to-anus distance was measured in the age of approximately 20 weeks. *Mc4r*$^{X16/X16}$ knock-in mice were significantly longer compared with *Mc4r*$^{wt/wt}$ mice (Figures 4a and b). As observed for the body weight phenotype, the effect on linear growth was intermediate in heterozygous Mc4r$^{X16/wt}$ animals. The effect size of the W16X stop mutation on body length was similar in both sexes approximately with 5% per *Mc4r*^{X16} allele.

Energy intake, energy assimilation and assimilation efficiency

Energy intake, energy assimilation (defined as the amount of energy resorbed by the intestine epithelium) and assimilation efficiency of 20-week-old mice were measured by bomb calorimetry. Hyperphagia in *Mc4r*$^{X16/X16}$ knock-in mice resulted in an increased energy intake (E_{in}) and energy assimilation (E_{ass}) in males as well as in females (Figures 5a–d). Assimilation efficiency was unaffected (Figures 5e and f). Heterozygous *Mc4r*$^{X16/wt}$ mutants exhibited no intermediate phenotype. Their energy intake and assimilation was similar to wild-type controls.

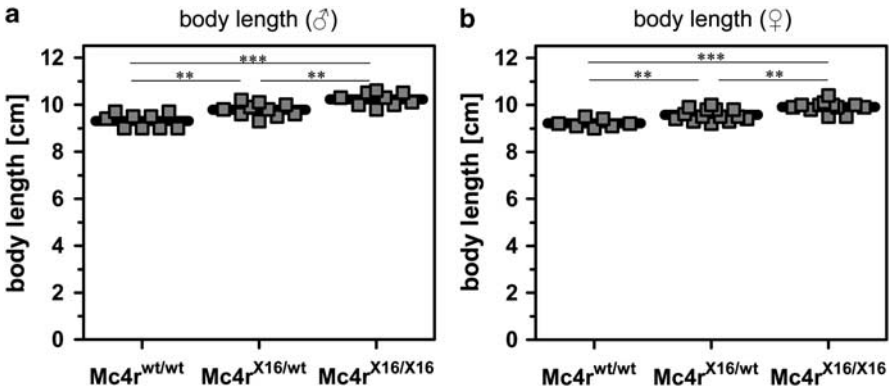

Figure 4 Body length of the *Mc4r*^{X16} knock-in mouse line. Body length of males ($n=9$–10) (**a**) and females ($n=7$–14) (**b**) at the age of approximately 20 weeks. Each dot represents the snout-to-anus distance of one individual animal (**$P<0.01$; ***$P<0.001$, one-way analysis of variance (ANOVA) and Holm–Sidak *post-hoc* test).

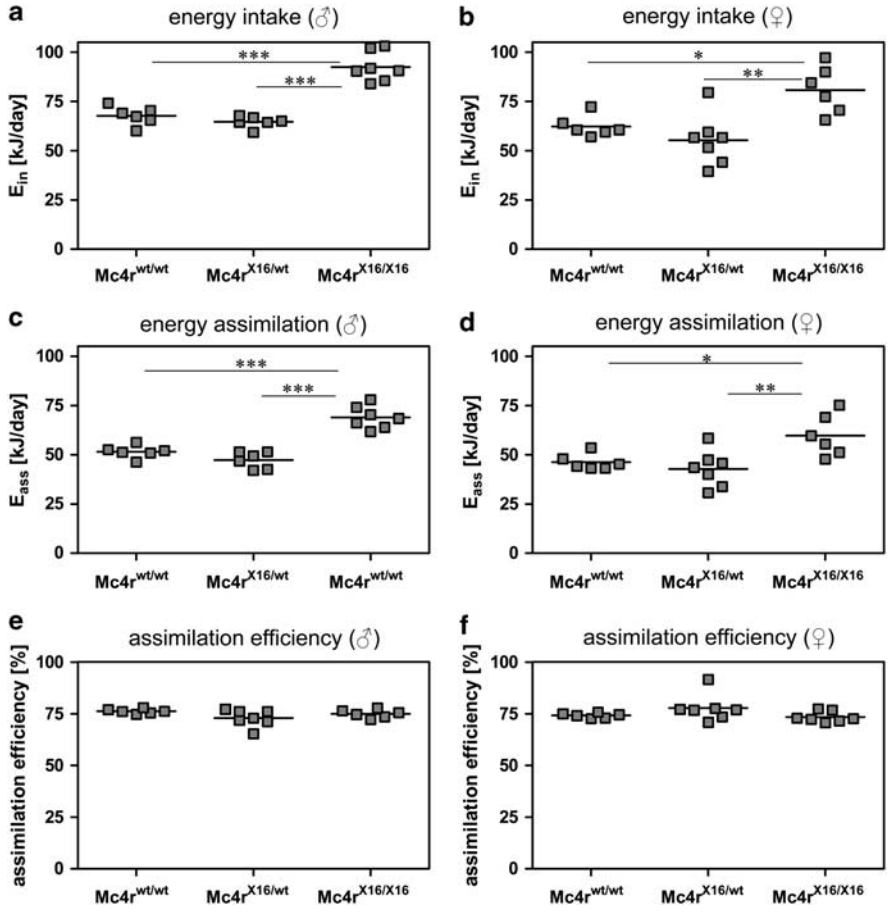

Figure 5 Energy intake (E_{in}), energy assimilation (E_{ass}) and assimilation efficiency. Food intake and feces production was monitored in mice singly housed for the duration (1 week) of the experiment. Food and feces samples were analyzed for their energy content by bomb calorimetry. Energy intake of male (**a**) and females (**b**) mice. Energy assimilation of male (**c**) and females (**d**) mice. Assimilation efficiency of male (**e**) and females (**f**) mice. Each dot represents one individual animal ($n=6$–7). (*$P<0.05$; **$P<0.01$; ***$P<0.001$, one-way analysis of variance (ANOVA) and Holm–Sidak *post-hoc* test).

Indirect calorimetry and body temperature

A second cohort of mice was used to determine daily energy expenditure by indirect calorimetry in an open flow system. During the measurements, *Mc4r*$^{X16/X16}$ mutants were heavier compared with *Mc4r*$^{wt/wt}$ mice. No difference in metabolic rate between genotypes was observed at the age

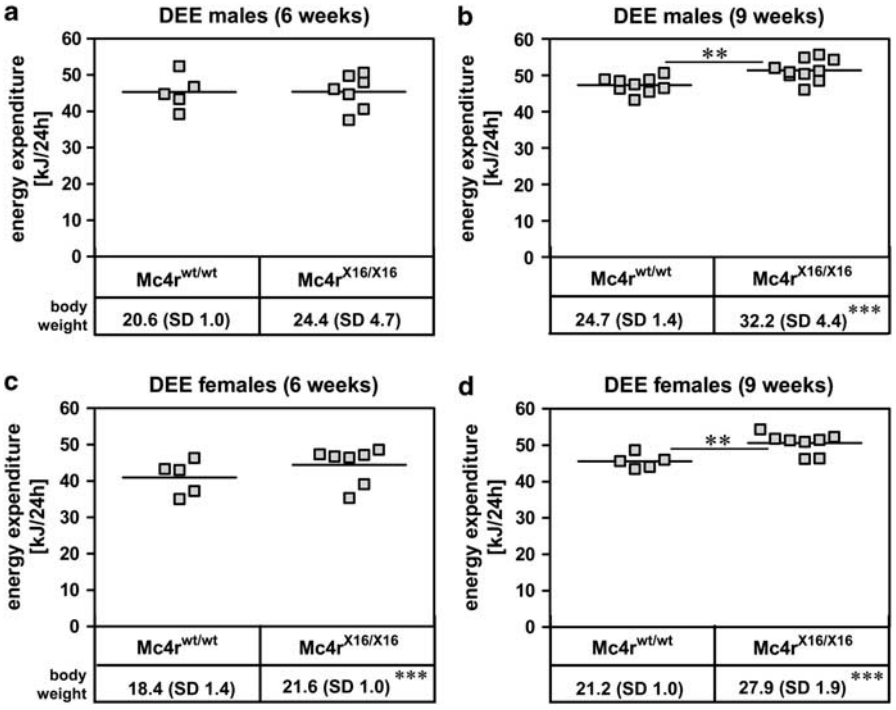

Figure 6 Daily energy expenditure (DEE). Indirect calorimetry was used to determine metabolic rates of *Mc4r*$^{wt/wt}$ and *Mc4r*$^{X16/X16}$ mice. Animals were housed 3 days in metabolic cages. Energy expenditure per animal for males ($n=5$–7) (**a**) and females ($n=5$–7) (**b**) in the age of 6 weeks; males ($n=9$–10) (**c**) and females ($n=5$–8) (**d**) in the age of 9 weeks. Each dot represents the value for one individual animal. Numbers below genotypes indicate body weight of the respective group with s.d. (**$P<0.01$; ***$P<0.001$, Student's *t*-test).

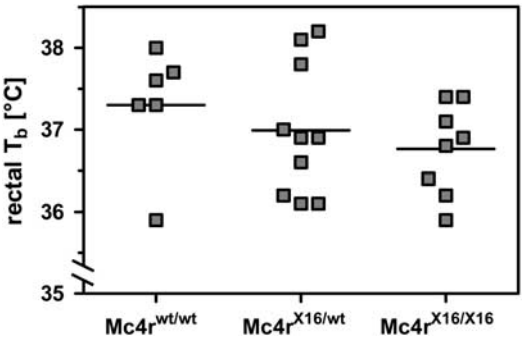

Figure 7 Body temperature of male mice in the age of around 20 weeks. Body temperature was assessed by a precision thermometer with a rectal probe. Measurements were performed always at the same time of day (around 1100 hours). Each dot represents one individual animal ($n=6$–10).

of 6 weeks (Figures 6a and b). At the age of 9 weeks, obese *Mc4r*$^{X16/X16}$ of both sexes had a significant elevated daily energy expenditure compared with *Mc4r*$^{wt/wt}$ mice (Figures 6c and d). Respiratory quotient was unchanged between genotypes (data not shown).

At the age of 20 weeks, body temperature of male mice was determined with a rectal probe. No significant difference appeared between the three genotypes, but a slight trend toward a lowered rectal body temperature was seen in *Mc4r*$^{X16/X16}$ and *Mc4r*$^{X16/wt}$ mutants in contrast to *Mc4r*$^{wt/wt}$ controls (Figure 7).

Hypothalamic gene expression

Expression of genes involved in the hypothalamic regulation of energy homeostasis was investigated in male mice at the age of 25–28 weeks by quantitative real-time PCR (Figure 8). The orexigenic genes *Npy* and *Agrp* displayed a significant downregulation in *Mc4r*$^{X16/X16}$ animals. In contrast, the anorexigenic *Pomc* was upregulated in mutant mice. *Mc4r* transcript abundance in mutant *Mc4r*$^{X16/X16}$ mice was significantly increased compared with wild-type littermates.

Intraperitoneal glucose tolerance test

Obesity is often accompanied by impaired glucose homeostasis.[15] Here, we performed an intraperitoneal glucose tolerance test in 6-h food deprived mice at the age of 20 weeks. *Mc4r*$^{X16/X16}$ of both sexes showed an impaired glucose clearance compared with *Mc4r*$^{X16/wt}$ and *Mc4r*$^{wt/wt}$ littermates resulting in an increased area under the curve. The effect was more pronounced in male mutants (Figure 9).

Aminoglycoside treatment

Owing to putative severe side effects of G-418,[33] in a first therapeutic trial we tested whether subcutaneous gentamicin and amikacin injections can alleviate obesity of *Mc4r*$^{X16/X16}$ knock-in mice. Both aminoglycosides were published as potent nonsense suppressors *in vivo* without evoking adverse effects.[5,7]

Male *Mc4r*$^{X16/X16}$ and *Mc4r*$^{wt/wt}$ mice in the age of 36 weeks were adapted to the handling by saline injections for 2 days. Hereafter, all mice received 34 mg kg^{-1} day^{-1}

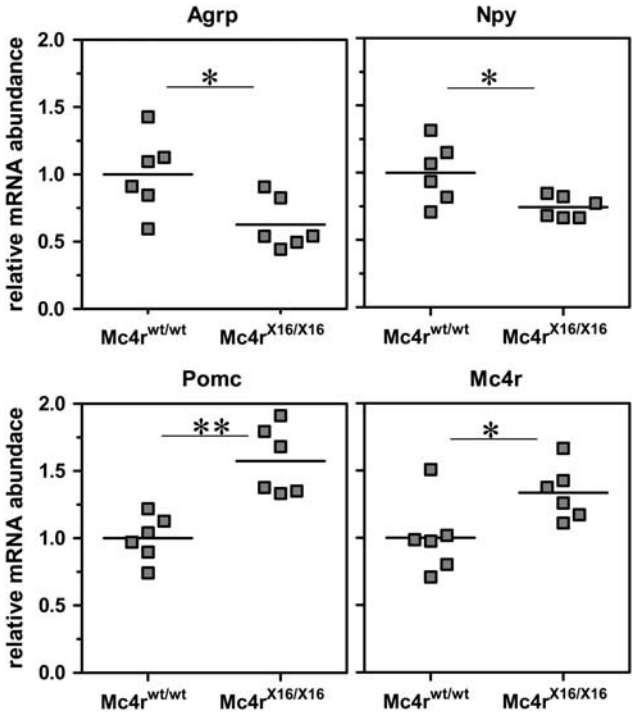

Figure 8 Hypothalamic gene expression in male mice in the age of approximately 6 months. RNA was extracted from hypothalamic tissue and transcripted into complementary DNA (cDNA). Quantification of genes involved in the control of energy balance was assessed by quantitative real-time PCR. Values were normalized against Hsp90 and β-actin. Each dot represents relative mRNA abundance for one individual mouse ($n=6$). (*$P<0.05$; **$P<0.01$, Mann–Whitney *U*-test).

gentamicin 1 h before the dark phase. No amelioration of obesity was observed during the 7-day gentamicin treatment. Both genotypes showed a slight reduction in body weight (~3%) (Figures 10a and b).

In a next step, we tested amikacin in adult *Mc4r*$^{X16/X16}$ and *Mc4r*$^{wt/wt}$ females at the age of 42 weeks. In the pretreatment phase, mice were adapted to handling by daily PBS injections for 1 week. Hereafter, all mice received 170 mg kg^{-1} day^{-1} amikacin. After 13 days, we increased the dose to 510 mg kg^{-1} day^{-1}. No reduction of obesity was observed during the treatment period (Figures 11a and b). The treatments were well tolerated by the mice.

Discussion

Nonsense suppressors such as aminoglycosides have the property to induce a read-through at premature termination codons leading to a partial rescue of protein expression. Up to now published studies did not address obesity-associated stop mutations as targets for nonsense mutation bypass therapy. To close this gap, we focused on the human obesity-associated MC4R stop mutation W16X.[21] We inserted the stop mutation into the murine *Mc4r* gene and studied the function of *Mc4r*^{X16} in a cell culture-based *in vitro* system. In addition, we established a new *Mc4r*^{X16} knock-in mouse line by gene targeting for the *in vivo* characterization of the nonsense allele.

As expected, heterologous overexpression in cell cultures demonstrated that MC4R^{X16} had a total loss-of-function phenotype. The truncated receptor consisting only of 15

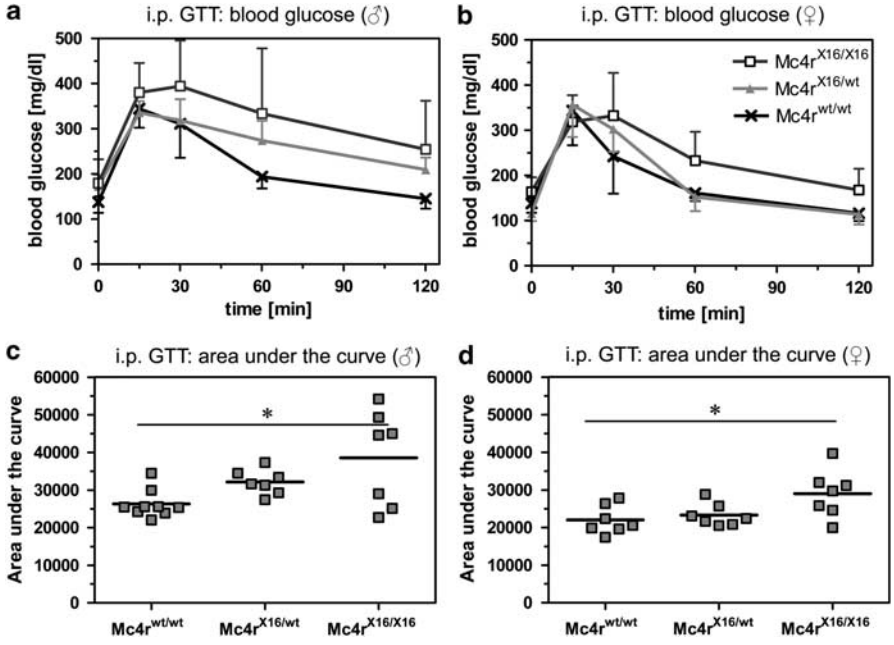

Figure 9 Intraperitoneal (i.p.) glucose tolerance test (GTT) of the *Mc4r*^{X16} knock-in mouse line in the age of 20 weeks. Animals were fasted for 6 h. After sampling blood from the tail for the determination of basal glucose concentration animals received and intraperitoneal glucose load (2 g kg^{-1}). Afterward blood was taken in regularly intervals. Blood glucose progression of male (**a**) and female (**b**) mice ($n=7$–9). Each point represents the mean value with s.d. The total area under the curve was calculated for each individual indicated by dots. Area under the curve for male (**c**) and female (**d**) mice ($n=7$–9). (*$P<0.05$, one-way analysis of variance (ANOVA), Tukey's *post-hoc* test).

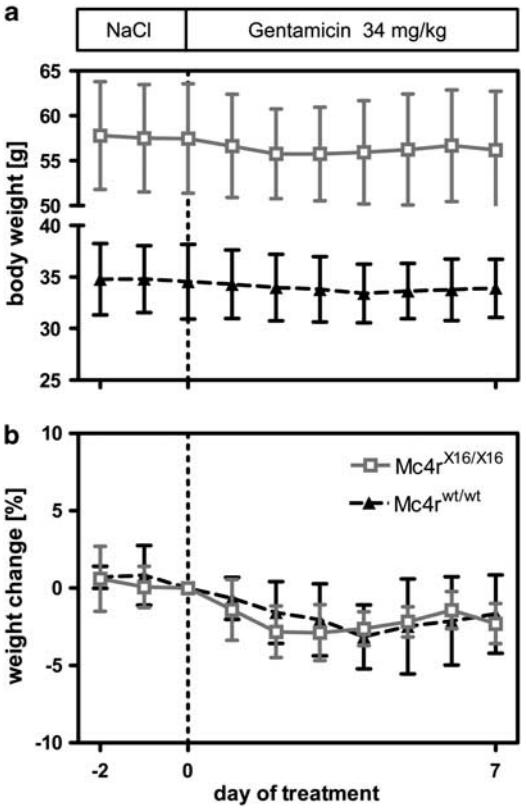

Figure 10 Subcutaneous injection of the aminoglycoside gentamicin in male mice at the age of 36 weeks. Grouply housed *Mc4r*$^{wt/wt}$ ($n=4$) and *Mc4r*$^{X16/X16}$ mice ($n=4$) were adapted for 2 days to the handling procedure by NaCl injections (day −2 to day 0). At day 0, all animals received once daily a single gentamicin injection in the indicated dose for 7 days. During the treatment period, body weight (**a**) was monitored. Body weight change displayed in percentage (**b**). Each point represents the mean value with s.d.

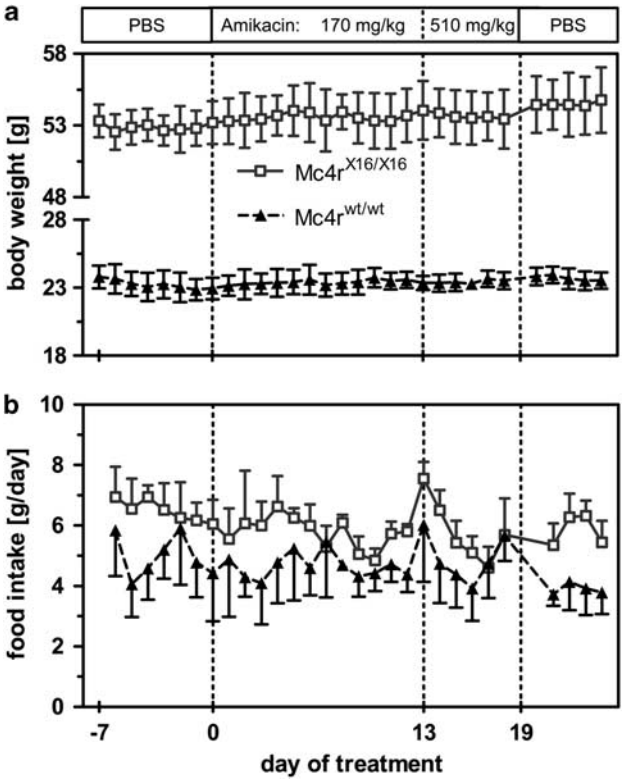

Figure 11 Subcutaneous injection of the aminoglycoside amikacin in female mice at the age of 42 weeks. Singly housed *Mc4r*$^{wt/wt}$ ($n=5$) and *Mc4r*$^{X16/X16}$ mice ($n=4$) were adapted for 1 week to the handling procedure by phosphate-buffered saline (PBS) injections (day −7 to day 0). At day 0, all animals received once daily a single amikacin (in PBS) injection in the indicated dose for 19 days. At day 19, all animals were switched back to PBS. During the treatment, body weight (**a**) and food intake (**b**) was monitored. Each point represents the mean value with s.d.

amino acids was not localized in its native compartment the plasma membrane. The endogenous agonist α-MSH and the superpotent artificial agonist NDP-α-MSH failed to promote cAMP-accumulation in cells expressing the *Mc4r*^{X16} gene. Nonsense suppression efficiencies depend on the sequence of the stop codon and the nucleotide context surrounding it. The W16X mutation generates a premature TGA termination codon with adenine in the 3′ position. This TGA A tetranucleotide sequence was effectively suppressed in other genes by aminoglycosides such as G-418, gentamicin and amikacin.[6,8] Here, we demonstrated that the incubation of *Mc4r*^{X16} transfected cells with G-418 restored receptor expression in the plasma membrane. Additionally, G-418 triggered a regain of agonist responsivity in *Mc4r*^{X16}-expressing cells. In cell culture experiments monitoring different receptor properties, we clearly demonstrated that the *Mc4r*^{X16} allele *per se* is a susceptible target to nonsense suppression. Recently, we published an article regarding aminoglycoside-mediated rescue of four different stop mutations in the human *MC4R* gene *in vitro* including W16X.[34] Consistently W16X in the human MC4R showed a similar susceptibility to aminoglycoside-mediated nonsense suppression most likely due to the fact that the nucleotide context (±6 bp) surrounding codon 16 is identical among mouse and human. For the evaluation of a therapeutic approach based on nonsense suppressors *in vivo*, we successfully generated an adequate *Mc4r*^{X16} knock-in mouse model by homologous recombination in ES cells. First, we investigated the metabolic profile of the knock-in mouse line. As anticipated homozygous *Mc4r*$^{X16/X16}$ knock-in mice developed severe obesity compared with *Mc4r*$^{wt/wt}$ controls accompanied by impaired glucose tolerance. A typical characteristic of mice carrying *Mc4r*^{X16} was an increased linear growth. This phenotype is in line with other *Mc4r*-deficient mouse models.[27,35]

Quantification of abdominal body composition revealed that weight gain was due to an increase in visceral fat mass. Interestingly, differences in body composition were identified in the two cohorts used for this study, which might be explained by different housing conditions suggesting that environmental factors like pathogen status, gut microflora and single/group housing affect obesity symptoms of *Mc4r*-deficient mice.

As obesity is the consequence of a positive energy balance, we monitored energy intake and energy assimilation as well as body temperature and energy expenditure. Homozygous mutants had a higher energy intake and assimilation than wild-type mice. The assimilation efficiency was unaffected demonstrating that increased energy assimilation is solely due to hyperphagia and not to a nutrient resorption abnormality in mutant mice.

Several studies demonstrated that MC4R agonists not only inhibit energy intake but also stimulate energy expenditure.[25,26] In *Mc4r*-deficient mice, one should therefore expect a lowered metabolic rate. Previous studies, however, reported conflicting data on this issue.[26,36,37] The analysis of metabolic rates in obese animal models is complicated by the fact that the rate of energy expenditure increases as a function of body weight. There is an ongoing debate how to adjust for differences in body weights when comparing metabolic rates in lean and obese individuals.[38] We here aimed to circumvent this problem by analyzing energy expenditure in young pre-obese mice. Six-week-old $Mc4r^{X16/X16}$ mice had already started to increase body weight, but did not exhibit a corresponding rise in daily energy expenditure, suggesting that mutant mice have a hypometabolic phenotype. In mutant $Mc4r^{X16/X16}$ mice, body fat accumulation is favored if body mass increase is not matched by energy expenditure. At the age of 9 weeks, $Mc4r^{X16/X16}$ mutants had an elevated metabolic rate compared with $Mc4r^{wt/wt}$ mice as a consequence of the growing obese phenotype. Clarification whether this elevation in energy expenditure is proportional or lower than expected from increased body weight demands normalization procedures with larger sample sizes.[39]

As a surrogate marker for metabolic rate, we assessed rectal body temperature in 20-week-old mice and observed a trend toward a lowered body temperature in $Mc4r^{wt/X16}$ and $Mc4r^{X16/X16}$ mutants further suggesting lower energy allocation toward thermoregulation in Mc4r-deficient mice.

Determination of hypothalamic gene expression revealed differences among $Mc4r^{wt/wt}$ and $Mc4r^{X16/X16}$ mice. In the arcuate nucleus, *Pomc*, *Agrp* and *Npy* are mainly expressed in leptin responsive neurons.[40–42] The orexigenic genes, *Agrp* and *Npy*, were downregulated in $Mc4r^{X16/X16}$ mice, whereas mRNA abundance of the anorexigenic gene *Pomc* was increased. Counter regulation of *Agrp/Npy* and *Pomc* transcripts is a characteristic feature in *Mc4r*-deficient mutants and indicates a leptin-mediated shift toward a catabolic gene expression profile.[43,44] As AGRP and the POMC-derived agonist α-MSH target the MC4R, regulation of *Pomc* and *Agrp* mRNAs is ineffective to prevent obesity in the *Mc4r*-deficient knock-in mouse line. *Npy* downregulation is not sufficient to perpetuate a lean phenotype in $Mc4r^{X16/X16}$ mice.

A significantly increased *Mc4r* transcript abundance was observed in $Mc4r^{X16/X16}$ knock-in mice compared with the wild types. Transcripts harboring stop mutations are often sequestered by nonsense-mediated mRNA decay.[45] In a previous study, it has been explicitly demonstrated that stop mutated *Mc4r* transcripts are not degraded by nonsense-mediated mRNA decay.[46] The upregulation of *Mc4r* mRNA in homozygous $Mc4r^{X16/X16}$ knock-in mice can be explained by an autoregulatory mechanism. Chronic stimulation of central melanocortin receptors with the artificial agonist Melanotan II leads to a reduction of *Mc4r* transcript levels in hypothalamic tissue of mice.[47] If an agonist-induced MC4R hyperactivity can reduce mRNA abundance by an unknown pathway, an opposite regulation is likely in $Mc4r^{X16/X16}$ mice with disrupted receptor signaling. Increased levels of stop mutated transcript are of advantage for nonsense suppression: high $Mc4r^{X16}$ transcript levels might lead to the formation of a higher number of mRNA/ribosome complexes therefore generating targets for nonsense suppressors to a greater extent. Beside a putative autoregulatory mechanism explaining the $Mc4r^{X16}$ transcript upregulation, we cannot exclude an effect of the remaining *loxP* sequence on mRNA levels.

Heterozygous $Mc4r^{wt/X16}$ mutants had an intermediate phenotype concerning body weight, body composition and longitudinal growth compared with wild-type and homozygous $Mc4r^{X16/X16}$ knock-in animals. These intermediate differences are in concordance with data from other Mc4r-deficient mouse lines and denote a dose dependency of MC4R signaling on metabolic parameters.[27,48] Thus, a partial rescue of MC4R activity *in vivo* could be of benefit to alleviate obesity symptoms of the $Mc4r^{X16}$ knock-in mouse line.

First, results using the aminoglycosides gentamicin and amikacin did not facilitate any amelioration of the obese phenotype of $Mc4r^{X16/X16}$ knock-in mice, although *in vivo* studies have demonstrated the nonsense suppressor potency of these aminoglycosides.[5,7,49] Several (interacting) factors can be responsible for the absence of a weight-reduction. We did not test amikacin in cell culture therefore it might be possible that the compound is *per se* ineffective on the W16X stop mutation explaining the result in the *in vivo* approach. On the other hand, gentamicin can reactivate $MC4R^{W16X}$ *in vitro*[34] but failed to do so *in vivo* suggesting other explanations for the absence of an anti-obesity effect of the administration. The protocol of aminoglycoside treatment is fundamental for the efficiency of nonsense suppression.[5] Hence, optimization of drug dosing/administration may be of benefit to reactivate $Mc4r^{X16}$ *in vivo*. Additionally, we cannot exclude a transient rescue of MC4R function in response to aminoglycosides on energy intake or energy expenditure, which would only be detectable during the first few hours after injection without affecting long-term energy balance. The aminoglycoside treatments were performed with adult mice when obesity is already severely developed. It seems worthwhile to explore the preventive therapeutic potential of nonsense suppression in younger pre-obese knock-in mice.

Several publications demonstrate a low penetration rate of gentamicin and amikacin across the blood–brain barrier.[50–52] The arcuate nucleus (ARC) of the hypothalamus is close to the median eminence, a circumventricular organ with an incomplete blood–brain barrier. Experiments with tracer substances suggest that neurons in the ARC

are located outside of the blood–brain barrier whereas hypothalamic areas with high levels of *Mc4r* expression like the paraventricular nucleus appear to be protected by the blood–brain barrier.[23,53] Until now, we did not perform pharmacokinetic studies but based on published observations amikacin/gentamicin concentrations in *Mc4r*-expressing sites after peripheral injections might be below effective concentrations because of the marginal penetration rate of aminoglycosides into brain tissue.

In future experiments, we will concentrate on optimization of aminoglycoside treatment protocols. Beside modifications of drug dosing, we will perform intracerebroventricluar canulations to directly supply *Mc4r*-expressing sites in the brain with nonsense suppressor drugs. Moreover, the application of non-aminoglycoside stop suppressors with other chemical properties such as negamycin and PTC124 appear promising to induce nonsense suppression *in vivo*.[12,14]

In summary, we demonstrated in cultured cells that the $Mc4r^{X16}$ allele is *per se* prone to aminoglycoside-mediated read-through. We therefore generated a $Mc4r^{X16}$ knock-in mouse line suitable for the *in vivo* evaluation of stop suppressor drugs. The mouse line showed a multitude of obesity symptoms that are perfectly in line with characteristics of other *Mc4r*-deficient animal models. Obesity as a quantitative trait is a simply accessible phenotype to evaluate nonsense suppression *in vivo*. In future experiments with the $Mc4r^{X16}$ knock-in mouse model will be instrumental to establish nonsense suppression for an obesity-associated target gene expressed in the central nervous system.

Conflict of interest

The authors declare no conflict of interest.

Acknowledgments

This work was supported by the Bundesministerium für Bildung und Forschung within the framework of the National Genome Research Network NGFN*plus* to Martin Klingenspor (01GS0822), Wolfgang Wurst (01GS0823) and to Heike Biebermann (01GS0825). We also would like to thank the BMBF/DLR for their support to Wolfgang Wurst (01GS0858).

References

1 Tsui LC. The spectrum of cystic fibrosis mutations. *Trends Genet* 1992; **8**: 392–398.
2 Scott HS, Litjens T, Nelson PV, Brooks DA, Hopwood JJ, Morris CP. Alpha-L-iduronidase mutations (Q70X and P533R) associate with a severe Hurler phenotype. *Hum Mutat* 1992; **1**: 333–339.
3 Wildin RS, Antush MJ, Bennett RL, Schoof JM, Scott CR. Heterogeneous AVPR2 gene mutations in congenital nephrogenic diabetes insipidus. *Am J Hum Genet* 1994; **55**: 266–277.
4 Prior TW, Bartolo C, Pearl DK, Papp AC, Snyder PJ, Sedra MS *et al.* Spectrum of small mutations in the dystrophin coding region. *Am J Hum Genet* 1995; **57**: 22–33.
5 Barton-Davis ER, Cordier L, Shoturma DI, Leland SE, Sweeney HL. Aminoglycoside antibiotics restore dystrophin function to skeletal muscles of mdx mice. *J Clin Invest* 1999; **104**: 375–381.
6 Manuvakhova M, Keeling K, Bedwell DM. Aminoglycoside antibiotics mediate context-dependent suppression of termination codons in a mammalian translation system. *RNA* 2000; **6**: 1044–1055.
7 Du M, Keeling KM, Fan L, Liu X, Kovacs T, Sorscher E *et al.* Clinical doses of amikacin provide more effective suppression of the human CFTR-G542X stop mutation than gentamicin in a transgenic CF mouse model. *J Mol Med* 2006; **84**: 573–582.
8 Keeling KM, Bedwell DM. Clinically relevant aminoglycosides can suppress disease-associated premature stop mutations in the IDUA and P53 cDNAs in a mammalian translation system. *J Mol Med* 2002; **80**: 367–376.
9 Mankin AS, Liebman SW. Baby, don't stop!. *Nat Genet* 1999; **23**: 8–10.
10 Hutchin T, Cortopassi G. Proposed molecular and cellular mechanism for aminoglycoside ototoxicity. *Antimicrob Agents Chemother* 1994; **38**: 2517–2520.
11 Mingeot-Leclercq MP, Tulkens PM. Aminoglycosides: nephrotoxicity. *Antimicrob Agents Chemother* 1999; **43**: 1003–1012.
12 Welch EM, Barton ER, Zhuo J, Tomizawa Y, Friesen WJ, Trifillis P *et al.* PTC124 targets genetic disorders caused by nonsense mutations. *Nature* 2007; **447**: 87–91.
13 Hirawat S, Welch EM, Elfring GL, Northcutt VJ, Paushkin S, Hwang S *et al.* Safety, tolerability, and pharmacokinetics of PTC124, a non-aminoglycoside nonsense mutation suppressor, following single- and multiple-dose administration to healthy male and female adult volunteers. *J Clin Pharmacol* 2007; **47**: 430–444.
14 Arakawa M, Shiozuka M, Nakayama Y, Hara T, Hamada M, Kondo S *et al.* Negamycin restores dystrophin expression in skeletal and cardiac muscles of mdx mice. *J Biochem* 2003; **134**: 751–758.
15 Kopelman PG. Obesity as a medical problem. *Nature* 2000; **404**: 635–643.
16 Hebebrand J, Hinney A. Environmental and genetic risk factors in obesity. *Child Adolesc Psychiatr Clin N Am* 2009; **18**: 83–94.
17 Hinney A, Schmidt A, Nottebom K, Heibult O, Becker I, Ziegler A *et al.* Several mutations in the melanocortin-4 receptor gene including a nonsense and a frameshift mutation associated with dominantly inherited obesity in humans. *J Clin Endocrinol Metab* 1999; **84**: 1483–1486.
18 Jackson RS, Creemers JW, Farooqi IS, Raffin-Sanson ML, Varro A, Dockray GJ *et al.* Small-intestinal dysfunction accompanies the complex endocrinopathy of human proprotein convertase 1 deficiency. *J Clin Invest* 2003; **112**: 1550–1560.
19 Krude H, Biebermann H, Schnabel D, Tansek MZ, Theunissen P, Mullis PE *et al.* Obesity due to proopiomelanocortin deficiency: three new cases and treatment trials with thyroid hormone and ACTH4-10. *J Clin Endocrinol Metab* 2003; **88**: 4633–4640.
20 Farooqi IS, Wangensteen T, Collins S, Kimber W, Matarese G, Keogh JM *et al.* Clinical and molecular genetic spectrum of congenital deficiency of the leptin receptor. *N Engl J Med* 2007; **356**: 237–247.
21 Marti A, Corbalan MS, Forga L, Martinez JA, Hinney A, Hebebrand J. A novel nonsense mutation in the melanocortin-4 receptor associated with obesity in a Spanish population. *Int J Obes Relat Metab Disord* 2003; **27**: 385–388.
22 Hinney A, Hohmann S, Geller F, Vogel C, Hess C, Wermter AK *et al.* Melanocortin-4 receptor gene: case-control study and transmission disequilibrium test confirm that functionally relevant mutations are compatible with a major gene effect for extreme obesity. *J Clin Endocrinol Metab* 2003; **88**: 4258–4267.
23 Mountjoy KG, Mortrud MT, Low MJ, Simerly RB, Cone RD. Localization of the melanocortin-4 receptor (MC4-R) in neuroendocrine and autonomic control circuits in the brain. *Mol Endocrinol* 1994; **8**: 1298–1308.
24 Smith AI, Funder JW. Proopiomelanocortin processing in the pituitary, central nervous system, and peripheral tissues. *Endocr Rev* 1988; **9**: 159–179.
25 Marsh DJ, Hollopeter G, Huszar D, Laufer R, Yagaloff KA, Fisher SL *et al.* Response of melanocortin-4 receptor-deficient mice to anorectic and orexigenic peptides. *Nat Genet* 1999; **21**: 119–122.
26 Chen AS, Metzger JM, Trumbauer ME, Guan XM, Yu H, Frazier EG *et al.* Role of the melanocortin-4 receptor in metabolic rate and food intake in mice. *Transgenic Res* 2000; **9**: 145–154.
27 Huszar D, Lynch CA, Fairchild-Huntress V, Dunmore JH, Fang Q, Berkemeier LR *et al.* Targeted disruption of the melanocortin-4 receptor results in obesity in mice. *Cell* 1997; **88**: 131–141.
28 Grosse J, Tarnow P, Rompler H, Schneider B, Sedlmeier R, Huffstadt U *et al.* N-ethyl-N-nitrosourea-based generation of mouse models

for mutant G protein-coupled receptors. *Physiol Genomics* 2006; **26**: 209–217.
29 Tao YX. The melanocortin-4 receptor: physiology, pharmacology, and pathophysiology. *Endocr Rev* 2010; **31**: 506–543.
30 Mul JD, van BR, Bergen DJ, Brans MA, Brakkee JH, Toonen PW *et al.* Melanocortin receptor 4 deficiency affects body weight regulation, grooming behavior, and substrate preference in the rat. *Obesity* 2011; doi:10.1038/oby.2011.81.
31 Eggan K, Akutsu H, Loring J, Jackson-Grusby L, Klemm M, Rideout III WM *et al.* Hybrid vigor, fetal overgrowth, and viability of mice derived by nuclear cloning and tetraploid embryo complementation. *Proc Natl Acad Sci USA* 2001; **98**: 6209–6214.
32 Heldmaier G, Ruf T. Body temperature and metabolic rate during natural hypothermia in endotherms. *J Comp Physiol B* 1992; **162**: 696–706.
33 La Rocca PT, Baker F, Frantz JD, Szot RJ, Black HE, Schwartz E. Skin and mucous membrane ulceration in beagle dogs following oral dosing with an experimental aminoglycoside antibiotic. *Fundam Appl Toxicol* 1985; **5**: 986–990.
34 Brumm H, Muhlhaus J, Bolze F, Scherag S, Hinney A, Hebebrand J *et al.* Rescue of Melanocortin 4 receptor (MC4R) nonsense mutations by aminoglycoside-mediated read-through. *Obesity* 2011; doi:10.1038/oby.2011.202.
35 Ollmann MM, Wilson BD, Yang YK, Kerns JA, Chen Y, Gantz I *et al.* Antagonism of central melanocortin receptors *in vitro* and *in vivo* by agouti-related protein. *Science* 1997; **278**: 135–138.
36 Ste ML, Miura GI, Marsh DJ, Yagaloff K, Palmiter RD. A metabolic defect promotes obesity in mice lacking melanocortin-4 receptors. *Proc Natl Acad Sci USA* 2000; **97**: 12339–12344.
37 Weide K, Christ N, Moar KM, Arens J, Hinney A, Mercer JG *et al.* Hyperphagia, not hypometabolism, causes early onset obesity in melanocortin-4 receptor knockout mice. *Physiol Genomics* 2003; **13**: 47–56.
38 Butler AA, Kozak LP. A recurring problem with the analysis of energy expenditure in genetic models expressing lean and obese phenotypes. *Diabetes* 2010; **59**: 323–329.
39 Kaiyala KJ, Morton GJ, Leroux BG, Ogimoto K, Wisse B, Schwartz MW. Identification of body fat mass as a major determinant of metabolic rate in mice. *Diabetes* 2010; **59**: 1657–1666.
40 Hakansson ML, Hulting AL, Meister B. Expression of leptin receptor mRNA in the hypothalamic arcuate nucleus—relationship with NPY neurones. *Neuroreport* 1996; **7**: 3087–3092.
41 Wilson BD, Bagnol D, Kaelin CB, Ollmann MM, Gantz I, Watson SJ *et al.* Physiological and anatomical circuitry between Agouti-related protein and leptin signaling. *Endocrinology* 1999; **140**: 2387–2397.
42 Cheung CC, Clifton DK, Steiner RA. Proopiomelanocortin neurons are direct targets for leptin in the hypothalamus. *Endocrinology* 1997; **138**: 4489–4492.
43 Tsuruta Y, Yoshimatsu H, Hidaka S, Kondou S, Okamoto K, Sakata T. Hyperleptinemia in A(y)/a mice upregulates arcuate cocaine- and amphetamine-regulated transcript expression. *Am J Physiol Endocrinol Metab* 2002; **282**: E967–E973.
44 Haskell-Luevano C, Schaub JW, Andreasen A, Haskell KR, Moore MC, Koerper LM *et al.* Voluntary exercise prevents the obese and diabetic metabolic syndrome of the melanocortin-4 receptor knockout mouse. *FASEB J* 2009; **23**: 642–655.
45 Hentze MW, Kulozik AE. A perfect message: RNA surveillance and nonsense-mediated decay. *Cell* 1999; **96**: 307–310.
46 Brocke KS, Neu-Yilik G, Gehring NH, Hentze MW, Kulozik AE. The human intronless melanocortin 4-receptor gene is NMD insensitive. *Hum Mol Genet* 2002; **11**: 331–335.
47 Zhang Y, Collazo R, Gao Y, Li G, Scarpace PJ. Intermittent MTII application evokes repeated anorexia and robust fat and weight loss. *Peptides* 2010; **31**: 639–643.
48 Meehan TP, Tabeta K, Du X, Woodward LS, Firozi K, Beutler B *et al.* Point mutations in the melanocortin-4 receptor cause variable obesity in mice. *Mamm Genome* 2006; **17**: 1162–1171.
49 Du M, Jones JR, Lanier J, Keeling KM, Lindsey JR, Tousson A *et al.* Aminoglycoside suppression of a premature stop mutation in a Cftr−/− mouse carrying a human CFTR-G542X transgene. *J Mol Med* 2002; **80**: 595–604.
50 Bruckner O, Alexander M, Martens F. Gentamicin concentrations in cerebrospinal fluid of patients with inflamed and uninflamed meninges (author's transl). *Infection* 1980; **8**: 86–89.
51 Briedis DJ, Robson HG. Cerebrospinal fluid penetration of amikacin. *Antimicrob Agents Chemother* 1978; **13**: 1042–1043.
52 Strausbaugh LJ, Brinker GS. Effect of osmotic blood-brain barrier disruption on gentamicin penetration into the cerebrospinal fluid and brains of normal rabbits. *Antimicrob Agents Chemother* 1983; **24**: 147–150.
53 Shaver SW, Pang JJ, Wainman DS, Wall KM, Gross PM. Morphology and function of capillary networks in subregions of the rat tuber cinereum. *Cell Tissue Res* 1992; **267**: 437–448.